Graphitic carbon nitride solid nanofilms for selective and recyclable sensing of Cu^{2+} and Ag^+

Heqin Huang, Rui Chen, Jiale Ma, Li Yan, Yingqi Zhao, Yu Wang, Wenjun Zhang, Jun Fan, Xianfeng Chen

Graphitic carbon nitride hybrid nanofilms are reported as sensitive, rapid and recyclable sensor for Cu^{2+} and Ag^+, and the sensing in serum demonstrates their potential in medical applications.

Journal Name
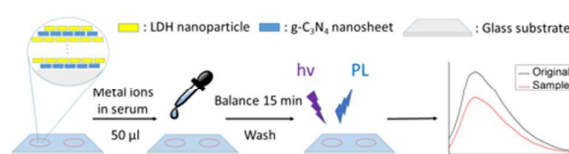
COMMUNICATION

Graphitic Carbon Nitride Solid Nanofilms for Selective and Recyclable Sensing of Cu^{2+} and Ag$^+$

Heqin Huang,[a,b] Rui Chen,[a,b] Jiale Ma,[a] Li Yan,[a,b] Yingqi Zhao,[a,b] Yu Wang,[a,b] Wenjun Zhang,[a,b] Jun Fan,*[a] Xianfeng Chen*[a,b]

Herein we report the fabrication of g-C$_3$N$_4$ nanofilms and their application as a solid fluorescence sensor. The as-prepared films are capable of convenient, sensitive, selective, rapid and recyclable sensing of Cu^{2+} and Ag$^+$ in water and serum, indicating the sensor's potential application in disease diagnosis. Attractively, our sensor is able to differentiate Cu^{2+} and Ag$^+$ by making use of their different adsorption and desorption kinetics during the interaction with g-C$_3$N$_4$ nanofilms.

Heavy metal ions receive great attention in medical examinations. These ions often play essential and important roles in living systems, but they may also possess toxicity and lead to severe health problems. For example, copper is a natural element in lives and plays a critical role in electron transition, and redox reactions in metalloenzyme.[1] In clinical practice, the blood copper concentration is utilized in the evaluation of copper metabolism. For human beings, the normal blood copper concentration is ranged from 100 to 150 μM/dl.[2] Abnormal copper content in body would be very damaging. Variation of copper concentration often indicates serious health problems. For instance, Menkes Kinky-Hair syndrome leads to a relatively lower copper concentration in blood.[3] Hodgkin's disease and Alzheimer's disease often raise blood copper contents.[4] Therefore, the change of blood copper concentration provides information for prediction and monitoring of these diseases. Furthermore, the blood copper contents of patients would change during the radiotherapy and chemotherapy, and this variation is an important evidence to evaluate the cancer treatment.[5] Except copper, silver and its compounds are also very important to human beings. For instance, silver and its compounds are extensively used in antibiotic devices; however, in some cases, silver is rapidly absorbed and cause hepatic, renal or neurologic toxicity.[6] Silver ions can interact with and displace certain metal ions like Ca^{2+} and Zn^{2+} in hydroxyapatite in bone.[7] Moreover, an excessive silver ion intake often leads to long-term accumulation of insoluble precipitates in the skin and eyes.[8] Therefore, similar to copper, blood silver is also useful indices of human silver exposure. With the importance of knowing the concentrations of Cu^{2+} and Ag$^+$, it is essential to have convenient and efficient technologies to monitor these metal ions in blood.

Presently, total reflection X-ray fluorescence (TXRF) spectroscopy allows fast, accurate and simultaneous analysis of all elements heavier than aluminium, and which is known as routine method of blood metal analysis. However, most existing TXRF systems are expensive and inconvenient in using.

Besides that, fluorescence metal ion probes, such as Organic dyes,[9] fluorescent metal probes[10] and quantum dots[11] receive much interest owing to their excellent sensitivity, versatility, device portability, low cost, and rapid response. However, these fluorescence sensors are still far from practical usage. Several inherent defects, such as high cost of rare metals, toxicity and complicate preparation limit their further development.

To address these problems, many new materials are being developed. Among them, graphitic carbon nitride (g-C$_3$N$_4$), the most stable allotrope of carbon nitride, attracts tremendous interests.[12] Metal-free g-C$_3$N$_4$ shows high photoluminescence (PL) intensity, good photostability, and excellent biocompatibility. All of these characteristics make g-C$_3$N$_4$ an ideal platform for catalysis,[13] bioimaging,[14] drug delivery[15] and sensing.[16] Lee *et al.* firstly reported cubic mesoporous-ordered g-C$_3$N$_4$ as a chemosensor of Cu^{2+} ions.[17] Recently, Tian *et al.*[18] and Zhang *et al.*[19] utilized exfoliated g-C$_3$N$_4$ nanomaterials as a turn-off fluorescence sensor for detection of Cu^{2+} and Fe^{3+} ions. However, in these reports, g-C$_3$N$_4$ was used in the form of aqueous solution, which is unfavourable for manipulation and cyclic utilization. Furthermore, the PL property of g-C$_3$N$_4$ is strongly affected by solvents and pH values. To improve this sensing platform, we propose to fabricate solid g-C$_3$N$_4$ films as the sensor.

Herein, for the first time, we fabricated g-C$_3$N$_4$ nanohybrid films as a fluorescence sensor. Layer-by-layer (LBL) self-assembly was employed to precisely control the growth of nanohybrid films of g-C$_3$N$_4$ and layered double hydroxides (LDH). Then, we investigated the sensitivity, kinetics and recyclability of the films for metal ion detection. The results show: (1) the detection limits of Cu^{2+} and Ag$^+$ are as low as 20 nM; (2) the films show faster response to Ag$^+$ and the Ag$^+$ quenched films can be more promptly recovered during washing; (3) the films are able to be repeatedly utilized for detection. Density function theory (DFT) calculations were performed to explain the different kinetics. Finally, the sensing tests were carried out in detecting the Cu^{2+} and Ag$^+$ in blood serum. The measurement proves that the proteins, peptides, lipids and carbohydrates show negligible influence to the sensing, which makes this technique an ideal method for diagnosis of certain severe diseases.

Graphitic C$_3$N$_4$ nanosheets were synthesized with sonication exfoliation of bulk g-C$_3$N$_4$ in water. Atomic force microscopy (AFM) images of g-C$_3$N$_4$ nanosheets in Figure 1 (a) and (b) reveal that the lateral diameter and thickness of the nanosheets are about 30 and 4-5 nm, respectively. In addition, Zeta potential test of g-C$_3$N$_4$ nanosheets display a -19.3 mV

surface charge in buffer-free aqueous solution. Figure S1 represents the XRD analysis of bulk g-C_3N_4 and exfoliated g-C_3N_4 nanosheets. After exfoliation, the peak at 13.3 degrees disappears. The remained peak at 27.6 degrees is corresponding to the interlayer distance of 0.32 nm, which is in line with the direct observation in the high resolution transmission electron microscopy image (Figure S2), and indicates the (002) peak of the layered aromatic system in g-C_3N_4 nanosheets. Furthermore, this interlayer distance suggests that 13-15 layers g-C_3N_4 nanosheets were obtained. Figure 1 (c) shows UV-Vis absorption and PL spectra of g-C_3N_4 nanosheets. The strongest absorption of UV-Vis spectrum appears at 315 nm, and the emission peak is at 442 nm in PL spectrum. The inset displays the g-C_3N_4 nanosheets solution under visible light and 365 nm irradiation. The g-C_3N_4 nanosheets solution emits clear blue fluorescent light under UV irradiation. Moreover, according to Figure S3, the strongest emission intensity occurs when excited at 330 nm.
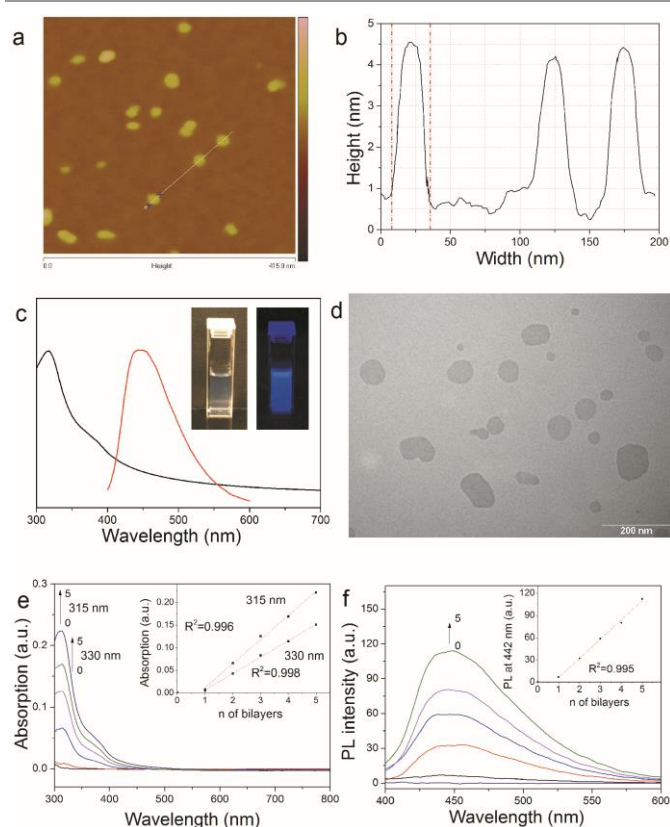

Figure 1. (a) AFM image of g-C_3N_4 nanosheets; (b) The corresponding height image of the three nanosheets shown in Figure 1 (a); (c) UV-Vis absorption and PL emission spectra of g-C_3N_4 nanosheets in water solution (black line: UV-Vis absorption; red line: PL emission), the insets indicate the g-C_3N_4 nanosheets solution under daylight (left) and 365 nm irradiation (right); (d) TEM image of well-dispersed Mg_2Al-Cl-LDH nanoparticles; (e) UV-Vis spectra of g-C_3N_4/LDH films (n=0-5) (inset: the linear relationship between the absorbance at 315 nm, 330 nm and n); (f) fluorescence spectra of g-C_3N_4/LDH films (n=0-5) (inset: the linear relationship between the PL intensity at 442 nm and n)

The Mg_2Al-Cl-LDH nanoparticles were prepared with a mean diameter of 50 nm and zeta potential of +40 mV in buffer-free aqueous solution. In Figure 1 (d), TEM observation shows the size and shape of well-dispersed LDH nanoparticles. The X-ray diffraction pattern in Figure S4 indicates the typical feature of pristine Mg_2Al-Cl-LDH nanoparticles, and the

diffraction peaks are corresponding to (003), (006) and (009) plane in LDH nanoparticles.

Mg_2Al-Cl-LDH nanoparticles and g-C_3N_4 nanosheets were utilized as building blocks in fabricating g-C_3N_4/LDH films via LBL self-assembly. In Figure 1 (e) and (f), the LBL self-assembly process was monitored by UV-Vis absorption and PL measurements. In Figure 1 (e), the strongest absorption of g-C_3N_4/LDH films occurs at 315 nm, which is corresponding to the characteristic absorption of g-C_3N_4 nanosheets. In PL measurement, 330 nm was utilized as the excitation wavelength, so in the UV-Vis spectra, these two wavelengths were recorded in the monitoring of self-assembly process. The inset graph of Figure 1 (e) indicates the monotonic increase of UV-Vis absorption from the first layer to fifth layer, which displays a uniform self-assembly process and demonstrates almost identical amounts of g-C_3N_4 nanosheets are incorporated in each growth cycle. The g-C_3N_4/LDH films also emit blue fluorescence light under UV irradiation. As shown in Figure 1 (f), the uniform growth of fluorescent intensities is in line with the stepwise deposition of g-C_3N_4 nanosheets. It is noted that the linear increase of absorbance and fluorescence of g-C_3N_4/LDH films starts from the second dipping of the substrates to g-C_3N_4. In contrast, the amount of the first g-C_3N_4 layer is very small. Observation of the self-assembly of the films with naked eyes also confirms the stepwise deposition of g-C_3N_4 during the g-C_3N_4/LDH bilayer growth. In Figure S5 (a), the photographs taken under UV irradiation display increased brightness along LBL self-assembly, revealing the enhanced blue luminescence upon increasing layers. In addition, the g-C_3N_4/LDH films show negligible loss of transparency in visible region, as shown in Figure S5 (b). Moreover, in Figure S6, SEM images display the microscopically and continuous films.

After we successfully prepared solid g-C_3N_4 nanofilms, their sensor application was explored. Firstly, we investigated the selectivity. In the experiment, g-C_3N_4/LDH films were treated with various types of metal ions, including Zn^{2+}, Al^{3+}, Cd^{2+}, Li^+, Ni^{2+}, Hg^+, Mg^{2+}, Ag^+, Cu^{2+}, Cr^{3+}, Fe^{3+}, Pb^{2+} and Co^{2+} (500 μM), and the results are present in Figure 2 (a). It can be found that the fluorescent intensities of the films were only dramatically quenched by Cu^{2+} and Ag^+, while other metal ions displayed insignificant influence. This selective quenching effect is owing to two reasons. Firstly, as shown in Figure S7, the N 1s XPS spectrum of g-C_3N_4/LDH film displays that nitrogen element in the film mainly exist as C-N=C (398.4 eV), C-N(-C)-C (399.3 eV) and C-NH_2, C-NH (400.3eV), while the C-N=C is dominant in g-C_3N_4.[20] All these functional groups exhibit high adsorption capacity to metal ions, especially Cu^{2+} and Ag^+ ions.[21] More importantly, the redox potentials of Cu^{2+} and Ag^+ lie between the conduction band and valence band of g-C_3N_4.[22] Hence, the photoinduced electron transfer (PET) from the conduction band of g-C_3N_4 to the Cu^{2+} and Ag^+ leads to fluorescence quenching. This aspect can be confirmed from XPS observation of the states of Cu^{2+} and Ag^+ in g-C_3N_4/LDH films. In Figure 2 (b), the Cu 2p XPS spectrum of the g-C_3N_4/LDH film treated by Cu ions solution shows a clear distribution of Cu^{2+} and Cu^+. The signals at 934.6 and 955.9 eV correspond to Cu^{2+} and the peaks at 932.6 and 952.5 eV are for Cu^+. The ratio of Cu^+ and Cu^{2+} is about 3.69, indicating most copper element in g-C_3N_4/LDH film exists as Cu^+. For Ag 3d XPS spectrum in Figure 2 (c), the distribution of silver element is similar with that of copper. The peaks at 368.2 and 374.2 eV indicate Ag^+, while the signals at 367.6 and 378.2 eV are corresponding to Ag^0. The ratio of Ag^0/Ag^+ is about 6.08, showing the domination of Ag^0 in the film. Our measured bonding energies are in line with those in previous reports.[23]
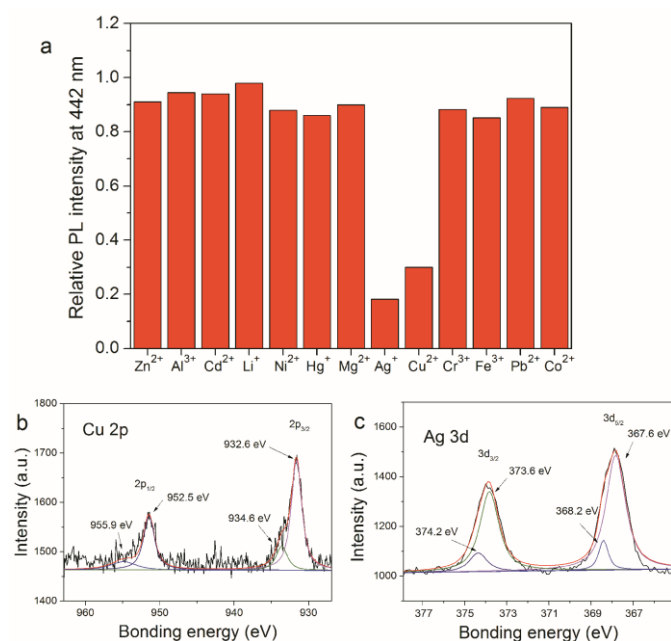
Figure 2. (a) The selective fluorescent response of g-C$_3$N$_4$/LDH films after treatment with 500 µM metal ions solution. (b) Cu 2p XPS spectrum of the g-C$_3$N$_4$/LDH film (treated by Cu^{2+}); (c) Ag 3d XPS spectrum of the g-C$_3$N$_4$/LDH film (treated by Ag$^+$).

Figure 3. PL spectra of g-C$_3$N$_4$/LDH films in the presence of (a) Cu^{2+} (from 20 nM to 5 mM) and (b) Ag$^+$ (from 20 nM to 500 µM); The fabricated films were quenched by (c) 10 µM Cu^{2+}, and (d) 1 µM Ag$^+$ and then washed in water for 48 hours. The procedures were repeated five times.

After we know that the films are sensitive to Cu^{2+} and Ag$^+$, the next question is how fast the response is. To investigate this, two g-C$_3$N$_4$ nanofilms were dipped separately into 5 mM Cu^{2+} and 500 µM Ag$^+$ solutions. The evolution of the PL intensities of the films with time is shown in Figure S8. It is apparent that the response of the films to Ag$^+$ is fast. The fluorescence is dramatically quenched in 500 µM Ag$^+$ within only 2 minutes and the quenching is saturated within 5 minutes. In comparison, the quenching of the films in 5 mM Cu^{2+} is a gradual process and it takes about 15 minutes to reach quenching saturation.

Once the required time for sensing is determined, we next investigate the sensitivity of the technique. For this, g-C$_3$N$_4$/LDH films were placed in Cu^{2+} and Ag$^+$ solutions of different concentrations. Figure 3 (a) and (b) shows that PL spectra of the films with the increase of Cu^{2+} and Ag$^+$ concentrations. Figure insets of Figure 3 (a) and (b) display the dependency of F/F$_0$ and the concentrations of Cu^{2+} and Ag$^+$, where F$_0$ and F are the fluorescence intensities at 442 nm in the absence and presence of metal ions. The fluorescence quenching are separated by a saturated concentration. At a range of low metal ions concentrations, PL intensities severely decrease until reach a value where fluorescence quenching saturates. The detection limits of g-C$_3$N$_4$/LDH films are 20 nM for both metal ions, which indicates a sensitive response to trace amounts of Cu^{2+} and Ag$^+$ in aqueous solutions.

For comparison, the sensitivity studies of dispersed g-C$_3$N$_4$ nanosheets in solution were also carried out with previous method (Figure S9).[18] It is clear that the solid g-C$_3$N$_4$ nanofilms present a similar quenching behaviour with free g-C$_3$N$_4$ nanosheets in solution. However, compared with the g-C$_3$N$_4$ nanosheets solution, the solid nanofilms are expected to be much more convenient for operation and storage. Another benefit is that the fluorescence of the quenched solid films can be easily recovered for repeated sensor application.
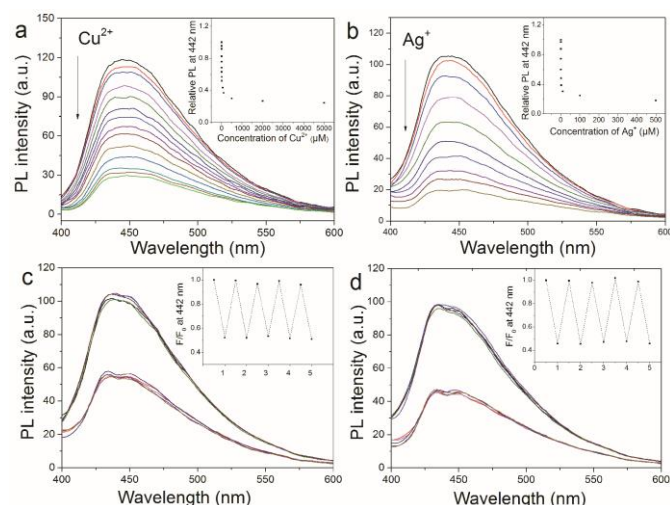
Figure 3 (c) and (d) show the variation of the luminescence intensities of g-C$_3$N$_4$/LDH films being quenchened by metal ions followed by washing with water. It can be observed that g-C$_3$N$_4$/LDH films show a readily reversible fluorescence change for at least 5 times. To speed up the recovery processes, the washing agent can be replaced by 1:1 acetonitrile/water solution. Since CN$^-$ possesses strong chelating effect to Cu^{2+} and Ag$^+$,[24] the fluorescence densities were recovered within 30 and 20 min, respectively for Cu^{2+} and Ag$^+$ (Figure S10). These results indicate the potential of g-C$_3$N$_4$/LDH films as a reusable luminescent sensor for Cu^{2+} and Ag$^+$.

From the results mentioned above, Cu^{2+} and Ag$^+$ display similar quenching effects to g-C$_3$N$_4$/LDH films, so a further technique is needed to distinguish them. According to previous work[20], glutathione, as a well-known metal ions chelating agent, shows negligible influence to the fluorescent properties of g-C$_3$N$_4$, so glutathione was applied to recover the quenched sensors. Attractively, eluting quenched films in glutathione solution can distinguish Cu^{2+} and Ag$^+$, which has not been reported before. As shown in Figure S11, the fluorescence of the films treated with Ag$^+$ is fully recovered within 30 min. However, with this short period of time, glutathione washing shows much lower assistance to the recovery of the fluorescence of the films treated with Cu^{2+}. Instead, the complete recovery of the Cu^{2+} quenched films require over 20 hours. To explain the different kinetics, we carried out density functional theory (DFT) calculations. The results are displayed in Figure S12 and S13. IS (IS'), TS (TS') and FS (FS') indicate the initial state, transition state and final state, respectively, of the adsorption process of Ag (Cu) to g-C$_3$N$_4$. In the initial state, ions are far away from g-C$_3$N$_4$ surface. In the final state, the ions have been adsorbed on the surface. With our calculations, the energy barriers of adsorption are 0.11 and 0.32 eV for Ag and Cu ion, respectively, and the corresponding backward energy barriers are 1.51 and 2.16 eV. The results indicate that the adsorption and desorption energy barriers in the Ag/g-C$_3$N$_4$ system are smaller than those of the Cu/g-C$_3$N$_4$ system (Figure S13 (b)). These results agree well with the experimental observations that Ag ions bind to (or dissociate from) g-C$_3$N$_4$ much more rapidly than Cu ions, i.e., g-C$_3$N$_4$ has faster response to Ag$^+$ than to Cu^{2+}.

Finally, in line with the fact that the concentration of Cu^{2+} and Ag^+ in blood is very important to the health of human beings. Following the scheme shown in Figure 4 (a), we demonstrated the sensing of metal ions in serum. In Figure 4 (b) and (c), PL intensities drop with the increase of Cu^{2+} and Ag^+ concentrations. The calibration curves indicate the linear relationship between Cu^{2+} concentrations and fluorescence quenching from 0 to 2.0 μM, while 0 to 200 nM for Ag^+. These results reveal that, in spite of the influence of proteins, peptides, lipid and carbohydrates in the serum, the sensing still well measures the slight variation of metal ion concentrations. Importantly, the sensing concentrations of Cu^{2+} is in line with the range for disease diagnosis and the fast and senstitive response to Ag^+ can help effective monitoring of human's exposure to sliver compounds. In the future, this technique can also be used for sensing these metal ions in urine for diagnosis.

Overall, our results imply that g-C_3N_4/LDH films are convenient, rapid, and sensitive sensor for monitoring blood copper and silver ions. In practice, for diagnosis, with this favourable technique, several diseases are likely to be diagnosed earlier or the outcome of certain therapies can be conveniently monitored.
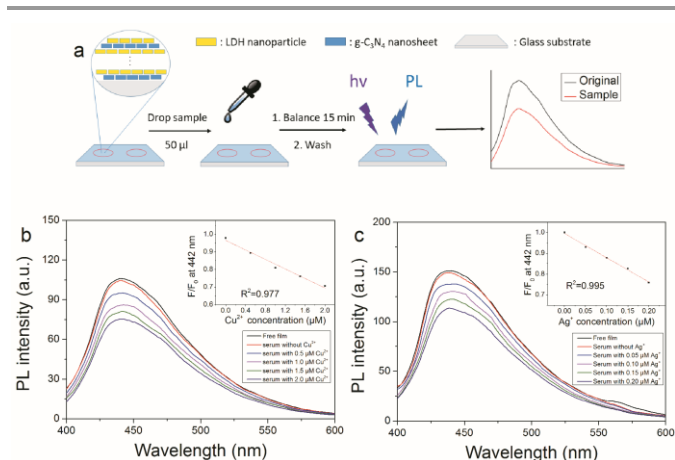

Figure 4. (a) Schematic representation of g-C_3N_4/LDH films for sensing of metal ions in serum. PL spectra of g-C_3N_4/LDH films in the presence of (b) Cu^{2+} and (c) Ag^+ in serum; insets display the dependence of F/F_0 on the concentrations of Cu^{2+} and Ag^+. (F_0 and F are the fluorescence intensities at 442 nm in the absence and presence of metal ions respectively).

Conclusions

In summary, we successfully fabricated g-C_3N_4/LDH nanohybrid films and demonstrated their applications in sensing Cu^{2+} and Ag^+ concentrations in aqueous solution and serum. The nanofilms are only sensitive to Cu^{2+} and Ag^+ and possess a low detection limitation of 20 nM for both ions. The quenched films can be easily recovered and reused for sensing. The nanofilms show faster response to Ag^+ and the Ag+ quenched films can be recover more quickly. Making use of this different kinetics, our technology can distinguish Cu^{2+} and Ag^+ by washing the quenched films in glutathione solution. DFT calculations were performed to explain the varied kinetics. The calculation results reveal that the adsorption and desorption energy barriers in the Ag/g-C_3N_4 system are smaller than those of the Cu/g-C_3N_4 system. The sensing of Cu^{2+} and Ag^+ in serum indicates that this technique may be practically used for diagnosis of certain severe diseases.

Notes and references

[a] Department of Physics and Materials Science, City University of Hong Kong, Hong Kong SAR, China. Fax: 852-34420538; Tel: 852-34427813; E-mail: xianfeng_chen@hotmail.com; junfan@cityu.edu.hk

[b] Center of Super-Diamond and Advanced Films (COSDAF), City University of Hong Kong, Hong Kong SAR, China.

1   H. Tapiero, D. M. Townsend, K. D. Tew, *Biomed. Pharmacother.,* 2003, **57**, 386.

2   H. S. Jung, P. S. Kwon, J. W. Lee, *J. Am. Chem. Soc.,* 2009, **131**, 2008.

3   S. G. Kaler, *Nat. Rev. Neurol.,* 2011, **7**, 15; I. Bertini, A. Rosato, *Cell. Mol. Life Sci.,* 2008, **65**, 89.

4   A. Kubala-Kukuś, D. Banaś, J. Braziewicz, *Biol. Trace Elem. Res.,* 2014, **158**, 22; R. Squitti, D. Lupoi, P. Pasqualetti, *Neurology,* 2002, **59**, 1153; G. J. Brewer, *Biofactors,* 2012, **38**, 107.

5   M. Zowczak, M. Iskra, L. Torliński, *Biol. Trace Elem. Res.,* 2001, **82**, 1.

6   S. Maitre, K. Jaber, J. L. Perrot, *Ann. Dermatol. Vener.,* 2002, **129**, 217.

7   J. F. Zhang, Y. Zhou, J. Yoon, *Chem. Soc. Rev.,* 2011, **40**, 3416.

8   P. L. Drake, K. J. Hazelwood, *Ann. Occup. Hyg.,* 2005, **49**, 575.

9   S. Sirilaksanapong, M. Sukwattanasinitt, P. Rashatasakhon, *Chem. Commun.,* 2012, **48**, 293; X. Yang, E. Wang, *Anal. Chem.,* 2011, **83**, 5005.

10 G. Lan, C. Huang, H. Chang, *Chem. Commun.,* 2010, **46**, 1257.

11 P. Yang, Y. Zhao, Y. Lu, *ACS nano,* 2011, **5**, 2147; A. Mandal, A. Dandapat, G. De, *Analyst,* 2012, **137**, 765.

12 P. Niu, L. Zhang, G. Liu, *Adv. Funct. Mater.,* 2012, **22**, 4763; S. Yang, Y. Gong, J. Zhang, *Adv. Mater.,* 2013, **25**, 2452.

13 N. Cheng, J. Tian, Q. Liu, *ACS Appl. Mater. Interfaces,* 2013, **5**, 6815; J. Tian, R. Ning, Q. Liu, *ACS Appl. Mater. Interfaces,* 2014, **6**, 1011; J. Tian, Q. Liu, A. M. Asiri, *ChemSusChem,* 2014, **7**, 2125.

14 X. Zhang, X. Xie, H. Wang, *J. Am. Chem. Soc.,* 2013, **135**, 18.

15 L. Lin, Z. Cong, J. Li, *J. Mater. Chem. B,* 2014, **2**, 1031.

16 S. Liu, J. Tian, L. Wang, *Adv. Mater.,* 2012, **24**, 2037; J. Tian, Q. Liu, C. Ge, *Nanoscale,* 2013, **5**, 8921; J. Tian, Q. Liu, C. Ge, *Nanoscale,* 2013, **5**, 11604.

17 E. Z. Lee, Y. Jun, W. H. Hong, *Angew. Chem. Int. Ed.,* 2010, **49**, 9706.

18 J. Tian, Q. Liu, A. M. Asiri, *Anal. Chem.,* 2013, **85**, 5595.

19 S. Zhang, J. Li, M. Zeng, *Nanoscale,* 2014, **6**, 4157.

20 Y. Tang, H. Song, Y. Su, *Anal. Chem.,* 2013, **85**, 11876.

21 Z. Li, L. Zhang, L. Wang, *Chem. Commun.,* 2011, **47**, 5798.

22 M. Merchán, T. S. Ouk, P. Kubát, *J. Mater. Chem. B,* 2013, **1**, 2139.

23 G. Z. Xing, J. B. Yi, J. G. Tao, *Adv. Mater.,* 2008, **20**, 3521; Q. Chen, W. Shi, Y. Xu, *Mater. Chem. Phys.,* 2011, **125**, 825; T. L. Freeman, S. D. Evans, A. Ulman, *Langmuir,* 1995, **11**, 4411.

24 E. Lee, S. Lee, N. Heo, *Chem. Commun.,* 2012, **48**, 3942.